

Aerosol sources during the 2013 North American biomass burning episode

G. Ancellet et al.

This discussion paper is/has been under review for the journal Atmospheric Chemistry and Physics (ACP). Please refer to the corresponding final paper in ACP if available.

Long range transport and mixing of aerosol sources during the 2013 North American biomass burning episode: analysis of multiple lidar observations in the Western Mediterranean basin

G. Ancellet¹, J. Pelon¹, J. Totems², P. Chazette², A. Bazureau¹, M. Sicard³, T. Di Iorio⁴, F. Dulac², and M. Mallet⁵

¹Sorbonne Université, UPMC, Université Versailles St-Quentin, CNRS/INSU, LATMOS, Paris, France

²LSCE, Laboratoire des sciences du Climat et de l'Environnement, CEA, Université Versailles St-Quentin, CNRS/INSU, Gif sur Yvette, France

³RSLab/CTE-CRAE-IEEC, Universitat Politècnica de Catalunya, Barcelona, Spain

⁴ENEA, Agenzia nazionale per le nuove tecnologie, l'energia e lo sviluppo economico sostenibile, Roma, Italy

⁵Laboratoire d'Aérodologie, Université Paul Sabatier, CNRS/INSU, Toulouse, France

Title Page

Abstract

Introduction

Conclusions

References

Tables

Figures



Back

Close

Full Screen / Esc

Printer-friendly Version

Interactive Discussion



Received: 9 October 2015 – Accepted: 30 October 2015 – Published: 18 November 2015

Correspondence to: G. Ancellet (gerard.ancellet@upmc.fr)

Published by Copernicus Publications on behalf of the European Geosciences Union.

ACPD

15, 32323–32365, 2015

**Aerosol sources
during the 2013 North
American biomass
burning episode**

G. Ancellet et al.

Title Page

Abstract

Introduction

Conclusions

References

Tables

Figures



Back

Close

Full Screen / Esc

Printer-friendly Version

Interactive Discussion



Abstract

Long range transport of biomass burning (BB) aerosols between North America and the Mediterranean region took place in June 2013. A large number of ground based and airborne lidar measurements were deployed in the Western Mediterranean during the Chemistry-AeRosol Mediterranean EXperiment (ChArMEx) intensive observation period. A detailed analysis of the potential North American aerosol sources is conducted including the assessment of their transport to Europe using forward simulations of the FLEXPART Lagrangian particle dispersion model initialized using satellite observations by MODIS and CALIOP. The three dimensional structure of the aerosol distribution in the ChArMEx domain observed by the ground-based lidars (Menorca, Barcelona and Lampedusa), a Falcon-20 aircraft flight and three CALIOP tracks, agree very well with the model simulation of the three major sources considered in this work: Canadian and Colorado fires, a dust storm from Western US and the contribution of Saharan dust streamers advected from the North Atlantic trade wind region into the Westerlies region. Four aerosol types were identified using the optical properties of the observed aerosol layers (aerosol depolarization ratio, lidar ratio) and the transport model analysis of the contribution of each aerosol source: (I) pure BB layer, (II) weakly dusty BB, (III) significant mixture of BB and dust transported from the trade wind region (IV) the outflow of Saharan dust by the subtropical jet and not mixed with BB aerosol. The contribution of the Canadian fires is the major aerosol source during this episode while mixing of dust and BB is only significant at altitude above 5 km. The mixing corresponds to a 20–30 % dust contribution in the total aerosol backscatter. The comparison with the MODIS AOD horizontal distribution during this episode over the Western Mediterranean sea shows that the Canadian fires contribution were as large as the direct northward dust outflow from Sahara.

Aerosol sources during the 2013 North American biomass burning episode

G. Ancellet et al.

Title Page

Abstract

Introduction

Conclusions

References

Tables

Figures



Back

Close

Full Screen / Esc

Printer-friendly Version

Interactive Discussion



1 Introduction

Forest fires are a significant source of tropospheric aerosol particles at northern latitudes in Spring and Summer (Generoso et al., 2003; Warneke et al., 2009) and many studies project higher temperatures and longer growing season e.g. (Flannigan et al., 2009; Liu et al., 2014). The focus of biomass burning emission impact on the atmospheric composition is often on the effect of these fires on the aerosol distribution in North America and Siberia (Eck et al., 2009; Warneke et al., 2010). Long range transport of biomass burning plumes has been also recognized as a significant source of aerosol in the mid-latitude free troposphere over Europe (Müller et al., 2005; Fiebig et al., 2003). Air mass aging related to long range transport also leads to aerosol optical and chemical properties different from results obtained when looking at observations close to the fire region (Lioussé et al., 1995; Müller et al., 2007). As an example, the absorbing efficiency in the visible spectral range is known to significantly increase in case of internally mixed BC (coating with secondary compounds) compared to externally mixed BC (Schnaiter et al., 2005). So far little attention has been paid to the frequent mixing of dust and biomass burning (BB) aerosol occurring during their transatlantic long range transport while lidar data analysis has shown that such a mixing will likely modify the extinction to backscatter ratio (BER) and then the aerosol optical depth (AOD) (Cattrell et al., 2005; Gross et al., 2011). Results of Paris et al. (2010) also show that the solubility of iron is enhanced by the mixing with biomass burning aerosols, while aerosol deposition may influence the rate of nitrogen fixation by microorganisms, and subsequently the global carbon cycle (Guieu et al., 2014). Although episodic, such long-range transport of smoke aerosols over the Mediterranean can also impact the regional energy budget by changing the distribution of solar energy. Indeed, for an aged BB plume, Formenti et al. (2002) report a net shortwave radiative forcing over the sea (daytime average) up to -64 W m^{-2} , at the surface and up to -22 W m^{-2} , at the top of the atmosphere (for an AOD of 0.40 at 550 nm). The large concentration of absorbing material (BC particles) within smoke plumes leads to significant absorp-

Aerosol sources during the 2013 North American biomass burning episode

G. Ancellet et al.

Title Page

Abstract

Introduction

Conclusions

References

Tables

Figures



Back

Close

Full Screen / Esc

Printer-friendly Version

Interactive Discussion



Aerosol sources during the 2013 North American biomass burning episode

G. Ancellet et al.

Title Page

Abstract

Introduction

Conclusions

References

Tables

Figures



Back

Close

Full Screen / Esc

Printer-friendly Version

Interactive Discussion



tion of solar radiations within the atmospheric layer where smoke resides, that could perturb the relative humidity and temperature vertical profiles. In the framework of the Chemistry-Aerosol Mediterranean Experiment/Aerosol Direct Radiative Impact in the Mediterranean (ChArMEx/ADRIMED) experimental campaign, many aerosol lidar and aircraft measurements have been made in June–July 2013 in the Mediterranean region during a case of intense biomass burning transport from North America to Europe (Mallet et al., 2015; Chazette et al., 2015; Pelon et al., 2015). Only a few studies report such long-range transport observations from North America to Europe (Forster et al., 2001; Petzold et al., 2007) or even the eastern Mediterranean (Formenti et al., 2002).

The purpose of this paper is to analyze the transatlantic long range transport of BB and dust aerosol sources from North America during this period. The context of our study is described in Sect. 2 by describing the main characteristics of the summer 2013 BB episode in North America and the observation network considered for the analysis of the aerosol distribution in the Mediterranean region. The aerosol sources are identified using satellite observations and the transport of dust or BB plumes is calculated with the FLEXPART Lagrangian model (see Sect. 3). The aerosol lidar observations are discussed in Sect. 4, where the contribution of the different aerosol sources is assessed using the comparison of the spatial distribution of the layers with the FLEXPART model simulations (forward from the sources region and backward to calculate the potential emission sensitivity for each observed aerosol layers). The mixing between dust and BB plumes is mainly derived from the analysis of the aerosol layer optical properties. The Menorca and aircraft lidar observations during ChArMEx are thoroughly described in a companion paper (Chazette et al., 2015) submitted with this paper and in a paper in preparation for the same special issue by J. Pelon and coworkers.

Aerosol sources during the 2013 North American biomass burning episode

G. Ancellet et al.

Title Page

Abstract

Introduction

Conclusions

References

Tables

Figures

◀

▶

◀

▶

Back

Close

Full Screen / Esc

Printer-friendly Version

Interactive Discussion



product is also considered to estimate the horizontal extent of BB plume when large AOD > 0.3 is found near the spots with elevated FRP. Both MODIS instruments on Aqua and Terra are considered to derive the daily mean. When a CALIOP overpass is found near the MODIS BB plume, the lidar vertical cross section is used to specify the vertical extent of the MODIS BB plume.

For the dust aerosol sources, two main information sources were considered: (i) North American dust storms identified in the NAAPS (Navy Aerosol Analysis and Prediction System) Global Aerosol Model simulations and (ii) 0.5 μm AOD anomalies from the MODIS daily products. AOD streamers transported from the tropical Atlantic belt of elevated 0.5 μm AOD to the mid-latitudes are related to the transport of Saharan dust across the Atlantic. CALIOP overpasses near the AOD anomalies again provide the vertical extent of dust aerosol layers.

In this work we use the new CALIOP level-1 (L1) version 4.0 attenuated backscatter coefficients β_{1064} and β_{532} because they correspond to a better calibration of the lidar data. They are averaged using a 10 km horizontal resolution and a 60 m vertical resolution (Vaughan et al., 2012). Before making horizontal or vertical averaging, the initial 333 m horizontal resolution (1 km above the altitude 8.2 km) are filtered to remove the cloud layer contribution (Winker et al., 2009). This cloud mask makes use of the Version 3 level-2 (L2) cloud layer data products (Vaughan et al., 2009). Our scheme for distinguishing cloud and aerosol is described in Ancellet et al. (2014). Although the lidar ratio (BER^{-1}) is available from the CALIOP Version 3 L2 aerosol layer data products, it is often based on an aerosol classification algorithm (Omar et al., 2009). In our work the lidar ratio (LR) is recalculated by using the aerosol layer transmittance and the integrated attenuated backscatter in the aerosol layer following the method described in Young (1995). To reduce the error when using high horizontal resolution CALIOP profiles, β_{532} is averaged over 80 km to compute the plume transmittance whenever it is possible. The attenuated backscatter is then corrected for the molecular and aerosol attenuation using a forward Klett inversion before calculating the backscatter ratio $R(z) = (\beta_a + \beta_R)/\beta_R$ at 532 and 1064 nm using the CALIOP atmo-

Aerosol sources during the 2013 North American biomass burning episode

G. Ancellet et al.

Title Page

Abstract

Introduction

Conclusions

References

Tables

Figures

◀

▶

◀

▶

Back

Close

Full Screen / Esc

Printer-friendly Version

Interactive Discussion



spheric density model to calculate the β_R Rayleigh backscatter vertical profiles. The aerosol depolarization ratio δ_{532} is also calculated using the perpendicular- to the parallel plus perpendicular polarized aerosol backscatter coefficient. We have also derived the color ratio defined as the ratio of the aerosol backscatter coefficients at 1064 and 532 nm ($C_a(z) = \beta_{a1064}/\beta_{a532} = (R_{1064}(z) - 1)/[16(R_{532}(z) - 1)]$). The aerosol color ratio can be also written as $C_a(z) = 2^{-k}$, where k is an exponent depending on the aerosol microphysical properties (Cattrall et al., 2005). These two ratios are provided only for $R(z) > 1.3$ because the uncertainty on the depolarization and color ratios are large for weak aerosol layers. Whenever it is possible, the use of nighttime overpasses are preferred to improve the signal-to-noise ratio (SNR).

The transport of the aerosol sources is analyzed using the FLEXPART model version 8.23 (Stohl et al., 2002) driven by 6 hourly ECMWF analysis (T213L91) interleaved with operational forecasts every 3 h. The model is run using a forward simulation with a tracer released within a volume estimated from the satellite observations. The release time period ranges from 1–3 days according to the MODIS AOD observations. The total mass of the tracer emitted is estimated using the aerosol concentration given in the NAAPS Global Aerosol Model simulations and FLEXPART calculates the gridded tracer concentration in ng m^{-3} . Considering the uncertainty in the estimate of the emitted tracer mass, the tracer distribution in the ChArMEx domain is analyzed using a relative mass fraction between the emitted mass and the calculated mass within the model grid cell. A factor is applied to calculate this ratio in order to take into account on one hand the difference between the emission volume ($\approx 5 \times 10^5 \text{ km}^3$) and the grid cell volume of the tracer concentration field ($\approx 2 \times 10^3 \text{ km}^3$), and on the other hand, the time difference between the emission period (1–3 days) and the integration time (6 h) used for the calculation of the tracer gridded concentration. The relative mass fraction is 100 % when the air mass is advected above the $0.5^\circ \times 0.5^\circ$ grid cell chosen for the gridded concentration calculation, without dilution ($< 100\%$) or concentration ($> 100\%$) of the tracer.

the same period. A FLEXPART forward run with a Saharan dust tracer was made for a wide area over Northern Africa in the box (24–34.5° N, 0–10° E, 0–6 km) from 23 to 28 June.

The vertical layering of the Saharan dust tracer over the ChArMEx domain is shown on 28 June in Fig. 9. As expected for a nearby source, the relative mass fraction is very large (> 100 %). Although the dust outflow from Sahara is transported above Lampedusa, it remains south of 36.6° N between Lampedusa and Cagliari. No Saharan dust is expected above Menorca. The altitude of the dust plume is between 2.5 and 4.5 km because the uplifting in the westerly flow is very limited.

4 Aerosol observations in the Mediterranean basin

In this section, the ChArMEx aircraft or ground based lidar observations and the CALIOP vertical cross sections on 27 and 28 June are compared with the expected contributions of the different aerosol sources transported across the Atlantic.

4.1 Spatial distribution of the aerosol layers

Three nighttime CALIOP overpasses are suitable for a comparison with the different BB plumes: 27 June at –10° W and at 10° E, and 28 June at 0° W. The backscatter ratio $R(z)$ and the aerosol depolarization ratio δ_{532} are shown in Fig. 10 in the latitude range where cloud free sky made possible the observations of aerosol layers. The $R(z)$ values are larger than 3 in these layers. On 27 June, the layers are in the altitude range 5 to 7.5 km at 10° E while it is between 2 and 5 km at 10° W. In both cases low δ_{532} values (< 10 %) are found, showing that the plumes are not mixed with significant amount of dust (except at 10° W where δ_{532} may reach 10 % in some layers). These results are in good agreement with the characteristics of the Canadian fire plumes discussed in Sect. 3. Indeed it was found that the front edge of the plume was at 10° E on 27 June with an altitude range 4–7 km, while the tail is at –10° W in the altitude range 2–5 km

Aerosol sources during the 2013 North American biomass burning episode

G. Ancellet et al.

Title Page

Abstract

Introduction

Conclusions

References

Tables

Figures



Back

Close

Full Screen / Esc

Printer-friendly Version

Interactive Discussion



(see vertical cross section on 28 June in Fig. 5). Although the Colorado fires may be present in the 27 June CALIOP cross section at -10° W according to the FLEXPART simulations, the altitude range of the observed aerosol layers is not consistent with the influence of the Colorado BB plume which is expected at altitude above 5 km. On 28 June at 0° W, the CALIOP observations show also aerosol layers in the 3–5 km altitude range, with slightly higher depolarization ratio ($\approx 10\%$), but still in the range expected for biomass burning aerosol (Nisantzi et al., 2014). The altitude range is again in good agreement with a major role of the tail of the Canadian fire plume.

Several ground based lidar observations have also identified aerosol plumes possibly related to the transatlantic transport. The characteristics of the aerosol layers are summarized in Table 3. The Menorca lidar data are discussed in a companion paper by Chazette et al. (2015). An aerosol layer between 3–5 km seen in Menorca is quite similar to the CALIOP observations on 28 June. A second layer between 5–7 km is also seen in Menorca with a noticeable depolarization ($\delta_{355} > 12\%$). The upper layer is not seen by CALIOP because it is expected at latitudes higher than 40° N and is masked by overlaying clouds. In Menorca the vertical profiles of the water vapor mixing ratio were also measured during the night (Chazette et al., 2014) showing elevated mixing ratio $> 1 \text{ g kg}^{-1}$ above 5 km and values near 0.5 g kg^{-1} in the aerosol layer observed around 4 km. The time series of the Menorca lidar is also useful to estimate the horizontal range of BB plume. The plume is observed for 24 h from 27 June 00:00 UT to 28 June 12:00 UT and the wind speed at 4 km is between $30\text{--}40 \text{ km h}^{-1}$, therefore the plume zonal extent is of the order of 1200 km. It is very similar to the size of the Canadian tracer plume obtained in the FLEXPART simulations (15° longitude difference between the front edge and the tail).

As expected the Barcelona lidar detects similar features: a strong layer between 5–7 km with $\delta_{532} \approx 10\%$ and an optically thin layer between 3–5 km with $\delta_{532} < 10\%$. The spectral variation of the aerosol depolarization ratio between Barcelona and Menorca cannot be accurately estimated but is less than 1.5. It is consistent with a small influence of urban aerosol (Burton et al., 2012). When looking at the Lampedusa lidar

Aerosol sources during the 2013 North American biomass burning episode

G. Ancellet et al.

Title Page

Abstract

Introduction

Conclusions

References

Tables

Figures

◀

▶

◀

▶

Back

Close

Full Screen / Esc

Printer-friendly Version

Interactive Discussion



data at 35° N, a layer is seen between 2 and 4 km on 28 June which is influenced by the Saharan dust outflow discussed in Sect. 3 since $\delta_{532} \geq 30\%$, i.e. a value similar to other dust layers observed over Menorca during ChArMEx (Chazette et al., 2015).

The Lampedusa lidar measures aerosol layers in the 2–4 km altitude range on both days, but with very different optical characteristics. A dust layer with $\delta_{532} > 30\%$ on 28 June, 12:00 UT while a mixture of dust and BB aerosol is seen on 27 June from 08:00 UT to 16:00 UT. The aerosol layer seen by CALIOP on 27 June 01:00 UT near 36° N has optical characteristics close to the layer observed in Lampedusa on 27 June (Fig. 10), i.e. a depolarization between 10–15 % and LR between 50–55 sr.

The LNG airborne lidar data obtained during ChArMEx will be thoroughly discussed in a forthcoming paper by J. Pelon and co-workers. Here we will only consider the vertical structure of the aerosol layers observed on 28 June along the loop shown in Fig. 1. The 3 corresponding vertical cross sections of attenuated $R(z)$ at 532 nm are shown in Fig. 11. Three interesting regions can be identified:

- (A) the 38.2° N layer at 2–4 km on the Cagliari-Lampedusa section and at 11–14° E on the return section between Messina and Cagliari,
- (B) the upper altitude layer in the 4–6 km altitude range covering a southwest (36° N, 12° E)-northeast (39° N, 15° E) band, the width of which is of the order of 100 km,
- (C) a low altitude layer between 2–4 km south of 36° N which corresponds to the layer seen by the Lampedusa lidar.

The spatial distribution of the aerosol layers seen by the LNG lidar corresponds quite well with the position of North American BB plumes and the expected latitudinal extent of the Saharan dust calculated with the FLEXPART simulation in Sect. 3. Indeed the layer A is related to the tail of the Canadian BB plume. The layer B is also in the latitude range of the Canadian BB plume, possibly mixed with the Colorado BB plume present between Gibraltar and Messina (see Fig. 4). Layer A and B seen by the LNG airborne

**Aerosol sources
during the 2013 North
American biomass
burning episode**

G. Ancellet et al.

Title Page

Abstract

Introduction

Conclusions

References

Tables

Figures



Back

Close

Full Screen / Esc

Printer-friendly Version

Interactive Discussion



lidar on 28 June are also consistent with the superposition of two different aerosol layers seen above Menorca 24 h before. In layer B, $\delta_{355} \approx 10\%$, i.e. higher than the low values found in layer A ($\delta_{355} \leq 5\%$).

4.2 Aerosol source attribution

Although the comparison with the position of the FLEXPART tracer plumes can already help to attribute a specific source to the observed layers in the ChArMEx area, it can be further checked by calculating the potential emission sensitivity (PES) values by running the FLEXPART model in the backward mode for 10–11 days to identify the area where surface emissions may influence the observed aerosol structure seen by CALIOP, the Menorca ground based lidar and the LNG airborne instrument. The PES is given in s unit in order to be multiplied by model surface fluxes to produce concentrations at the receptor location. The PES is calculated using 6 h averages on a three dimensional $1^\circ \times 1^\circ \times 1$ km grid. The results are shown for the CALIOP and Menorca observations on 27 June (Fig. 12). Similar calculations were also made for layer A, B and C seen by the airborne lidar on 28 June (Fig. 13). The simulations for the layers seen by CALIOP on 28 June, 02:00 UT are not shown because they are very similar to the results obtain for the Menorca lidar on 27 June at 12:00 UT or for layer B seen by LNG.

The aerosol layers observed by CALIOP along the two cross sections at -10° W and 10° E are indeed mainly related to aerosol sources over Canada and Alaska, but the retro-plume altitude and latitude at 60° W are quite different when reaching the Atlantic Ocean. The probability of dust and biomass mixing is higher for the CALIOP layers at -10° W which is located in the 40 – 50° N latitude band at lower altitude (5–7 km) than for the CALIOP layers at 10° E. This may explain the slight depolarization difference for the two CALIOP tracks since there are more layers with $\delta_{532} \approx 10\%$ at -10° W than at 10° E. The mixing of Atlantic dust sources and Canadian BB aerosol is even more explicit for the Menorca layer at 6 km since two branches of elevated PES are seen over the two aerosol source regions identified for this layer. It explains the relatively higher

Aerosol sources during the 2013 North American biomass burning episode

G. Ancellet et al.

Title Page

Abstract

Introduction

Conclusions

References

Tables

Figures

◀

▶

◀

▶

Back

Close

Full Screen / Esc

Printer-friendly Version

Interactive Discussion



Aerosol sources during the 2013 North American biomass burning episode

G. Ancellet et al.

Title Page

Abstract

Introduction

Conclusions

References

Tables

Figures

◀

▶

◀

▶

Back

Close

Full Screen / Esc

Printer-friendly Version

Interactive Discussion



aerosol depolarization ratio (up to 12 %) at 6 km than at 4 km in Menorca during this episode. Such a transport pathway is also consistent with the water vapor mixing ratio maximum $> 1 \text{ g kg}^{-1}$ seen by the Menorca water vapor lidar near 6 km since uplifting of air masses from the lower troposphere above the Atlantic Ocean is likely to increase the humidity in the mid-troposphere.

When considering the PES related to the airborne lidar layers, the layer A PES is similar to the 10° E plume showing a strong influence of the Canadian aerosol BB source, while the layer B PES distribution resembles the results obtained with the Menorca layer seen one day earlier. For the dusty layer C seen both by the aircraft and at the Lampedusa station, the PES distribution shows that there is no transatlantic transport for the period 17 to 28 June while the aerosol sources are mainly located above North Africa and Western Europe at low altitude ($< 3 \text{ km}$). Although air masses are still advected from Western Europe, Saharan dust emission remains the major aerosol source since Western Europe air masses were heavily influenced by Saharan dust layers during the period 16 to 20 June (Mallet et al., 2015). It is consistent with the large depolarization seen both above Lampedusa ($\delta_{532} \approx 30 \%$).

The ATR42 aircraft also flew between Cagliari and Lampedusa on 28 June around 12:00 UT to sample the aerosol layers with in-situ measurements (Pelon et al., 2015). The analysis of the CO and BC in-situ measurements made on-board the ATR42 shows that the layer A and B correspond to a CO excess above background of the order of 100 ppbv while ΔCO is less than 20 ppbv for layer C (not shown). The BC variability shows also the same pattern. This is in very good agreement with the conclusions derived from the lidar data analysis coupled with the Lagrangian transport model simulations.

4.3 Aerosol optical properties

In this section, we will summarize the results about the aerosol layer optical properties and the aerosol source attribution. The analysis conducted in the previous sections

Aerosol sources during the 2013 North American biomass burning episode

G. Ancellet et al.

Title Page

Abstract

Introduction

Conclusions

References

Tables

Figures



Back

Close

Full Screen / Esc

Printer-friendly Version

Interactive Discussion



of the different aerosol source contributions when it is coupled with the results of the Lagrangian FLEXPART transport model. Four aerosol types were identified using the depolarization ratio and the three dimensional structure of the aerosol plume: (I) pure BB layer, (II) weakly dusty BB, (III) a significant mixture of BB and dust transported from the North Atlantic trade wind region (IV) the direct northward outflow by the subtropical jet of Saharan dust not mixed with BB aerosol. Mixing of dust and BB can correspond to a 20–30 % dust contribution in the total aerosol backscatter. The comparison with the MODIS AOD distribution during this episode over the Western Mediterranean sea shows that the Canadian fires contribution were surprisingly as large as the direct northward dust outflow from Sahara. An additional contribution from a mid-tropospheric aerosol layer due a mixture of dust and BB aerosol was found in the region of higher AOD seen by MODIS. The next step will now concern the use of all presented and analyzed data for evaluating 3-D regional models to simulate this specific event, in terms of optical properties, possible mixing and vertical extent of mineral dust and forest fire aerosol layers.

Acknowledgements. This work was funded by the French MISTRALS program funded by CNRS/INSU, ADEME, CEA, Météo-France and CNES for aerosol and cloud satellite missions validation. The NILU team lead by A. Stohl is gratefully acknowledged for distributing the FLEXPART model. The SAFIRE team, INSU DT and D. Bruneau from LATMOS are gratefully acknowledged for the aircraft flight operation and the LNG lidar operation. The lidar measurements in Barcelona were supported by the 7th Framework Programme project Aerosols, Clouds, and Trace Gases Research Infrastructure Network (ACTRIS) (grant agreement no. 262254) and by the Spanish Ministry of Science and Innovation and FEDER funds under the projects TEC2012-34575, UNPC10-4E-442 and CGL2011-13580-E/CLI.

References

Ancellet, G., Pelon, J., Blanchard, Y., Quennehen, B., Bazureau, A., Law, K. S., and Schwarzenboeck, A.: Transport of aerosol to the Arctic: analysis of CALIOP and French aircraft

**Aerosol sources
during the 2013 North
American biomass
burning episode**

G. Ancellet et al.

Title Page

Abstract

Introduction

Conclusions

References

Tables

Figures



Back

Close

Full Screen / Esc

Printer-friendly Version

Interactive Discussion

data during the spring 2008 POLARCAT campaign, *Atmos. Chem. Phys.*, 14, 8235–8254, doi:10.5194/acp-14-8235-2014, 2014. 32330

Brahney, J., Ballantyne, A., Sievers, C., and Neff, J.: Increasing Ca^{2+} deposition in the western US: the role of mineral aerosols, *Aeolian Res.*, 10, 77–87, 2013. 32333

5 Burton, S. P., Ferrare, R. A., Hostetler, C. A., Hair, J. W., Rogers, R. R., Obland, M. D., Butler, C. F., Cook, A. L., Harper, D. B., and Froyd, K. D.: Aerosol classification using airborne High Spectral Resolution Lidar measurements – methodology and examples, *Atmos. Meas. Tech.*, 5, 73–98, doi:10.5194/amt-5-73-2012, 2012. 32336, 32340

10 Catrall, C., Reagan, J., Thome, K., and Dubovik, O.: Variability of aerosol and spectral lidar and backscatter and extinction ratios of key aerosol types derived from selected Aerosol Robotic Network locations, *J. Geophys. Res.*, 110, D10S11, doi:10.1029/2004JD005124, 2005. 32326, 32331

15 Chazette, P., Marnas, F., and Totems, J.: The mobile Water vapor Aerosol Raman Lidar and its implication in the framework of the HyMeX and ChArMEX programs: application to a dust transport process, *Atmos. Meas. Tech.*, 7, 1629–1647, doi:10.5194/amt-7-1629-2014, 2014. 32329, 32336

20 Chazette, P., Totems, J., Ancellet, G., and Sicard, M.: Temporal consistency of lidar observables during aerosol transport events in the framework of the ChArMEX/ADRIMED campaign at Menorca Island in June 2013, *Atmos. Chem. Phys. Discuss.*, accepted, 2015. 32327, 32336, 32337, 32341

CIFFC: Canadian Interagency Forest Fire Center Inc. Report 2013, available at: http://www.ciffc.ca/images/stories/pdf/2013_canada_report.pdf, 2013. 32328

25 Di Iorio, T., di Sarra, A., Sferlazzo, D. M., Cacciani, M., Meloni, D., Monteleone, F., Fuá, D., and Fiocco, G.: Seasonal evolution of the tropospheric aerosol vertical profile in the central Mediterranean and role of desert dust, *J. Geophys. Res.-Atmos.*, 114, D02201, doi:10.1029/2008JD010593, 2009. 32329, 32341

30 Eck, T. F., Holben, B. N., Reid, J. S., Sinyuk, A., Hyer, E. J., O'Neill, N. T., Shaw, G. E., Vande Castle, J. R., Chapin, F. S., Dubovik, O., Smirnov, A., Vermote, E., Schafer, J. S., Giles, D., Slutsker, I., Sorokine, M., and Newcomb, W. W.: Optical properties of boreal region biomass burning aerosols in central Alaska and seasonal variation of aerosol optical depth at an Arctic coastal site, *J. Geophys. Res.-Atmos.*, 114, D11201, doi:10.1029/2008JD010870, 2009. 32326

Aerosol sources during the 2013 North American biomass burning episode

G. Ancellet et al.

Title Page

Abstract

Introduction

Conclusions

References

Tables

Figures



Back

Close

Full Screen / Esc

Printer-friendly Version

Interactive Discussion



- Fiebig, M., Stohl, A., Wendisch, M., Eckhardt, S., and Petzold, A.: Dependence of solar radiative forcing of forest fire aerosol on ageing and state of mixture, *Atmos. Chem. Phys.*, 3, 881–891, doi:10.5194/acp-3-881-2003, 2003. 32326
- Flannigan, M., Stocks, B., Turetsky, M., and Wotton, M.: Impacts of climate change on fire activity and fire management in the circumboreal forest, *Glob. Change Biol.*, 15, 549–560, doi:10.1111/j.1365-2486.2008.01660.x, 2009. 32326
- Formenti, P., Boucher, O., Reiner, T., Sprung, D., Andreae, M. O., Wendisch, M., Wex, H., Kindred, D., Tzortziou, M., Vasaras, A., and Zerefos, C.: STAAARTE-MED 1998 summer airborne measurements over the Aegean Sea 2. Aerosol scattering and absorption, and radiative calculations, *J. Geophys. Res.-Atmos.*, 107, 4451, doi:10.1029/2001JD001536, 2002. 32326, 32327
- Forster, C., Wandinger, U., Wotawa, G., James, P., Mattis, I., Althausen, D., Simmonds, P., O'Doherty, S., Jennings, S. G., Kleefeld, C., Schneider, J., Trickl, T., Kreipl, S., Jäger, H., and Stohl, A.: Transport of boreal forest fire emissions from Canada to Europe, *J. Geophys. Res.-Atmos.*, 106, 22887–22906, doi:10.1029/2001JD900115, 2001. 32327
- Generoso, S., Bréon, F.-M., Balkanski, Y., Boucher, O., and Schulz, M.: Improving the seasonal cycle and interannual variations of biomass burning aerosol sources, *Atmos. Chem. Phys.*, 3, 1211–1222, doi:10.5194/acp-3-1211-2003, 2003. 32326
- Ginoux, P., Chin, M., Tegen, I., Prospero, J. M., Holben, B., Dubovik, O., and Lin, S.-J.: Sources and distributions of dust aerosols simulated with the GOCART model, *J. Geophys. Res.-Atmos.*, 106, 20255–20273, doi:10.1029/2000JD000053, 2001. 32333
- Gross, S., Tesche, M., Freudenthaler, V., Toledano, C., Wiegner, M., Ansmann, A., Althausen, D., and Seefeldner, M.: Characterization of Saharan dust, marine aerosols and mixtures of biomass-burning aerosols and dust by means of multi-wavelength depolarization and Raman lidar measurements during SAMUM 2, *Tellus B*, 63, 706–724, doi:10.1111/j.1600-0889.2011.00556.x, 2011. 32326
- Gross, S., Geiss, A., Heimerl, K., Gasteiger, J., Freudenthaler, V., Weinzier, B., and Wiegner, M.: Characterization of long-range transported Canadian biomass burning over Central Europe – a case study, *Geophys. Res. Abstr.*, EGU General Assembly 2015, Vienna, Austria, 2561, 2015. 32333
- Guieu, C., Ridame, C., Pulido-Villena, E., Bressac, M., Desboeufs, K., and Dulac, F.: Impact of dust deposition on carbon budget: a tentative assessment from a mesocosm approach, *Biogeosciences*, 11, 5621–5635, doi:10.5194/bg-11-5621-2014, 2014. 32326

Aerosol sources during the 2013 North American biomass burning episode

G. Ancellet et al.

Title Page

Abstract

Introduction

Conclusions

References

Tables

Figures



Back

Close

Full Screen / Esc

Printer-friendly Version

Interactive Discussion



Hahnenberger, M. and Nicoll, K.: Meteorological characteristics of dust storm events in the eastern Great Basin of Utah, USA, *Atmos. Environ.*, 60, 601–612, doi:10.1016/j.atmosenv.2012.06.029, 2012. 32333

Kumar, D., Rocadenbosch, F., Sicard, M., Comeron, C., Munoz, C., Lange, D., Tomas, S., and Gregorio, E.: Six-channel polychromator design and implementation for the UPC elastic Raman LIDAR, in: *SPIE Remote Sensing*, p. 81820, International Society for Optics and Photonics, Prague, Czech Republic, 2011. 32329

Liousse, C., Devaux, C., Dulac, F., and Cachier, H.: Aging of savanna biomass burning aerosols: consequences on their optical properties, *J. Atmos. Chem.*, 22, 1–17, doi:10.1007/BF00708178, 1995. 32326

Liu, Y., Goodrick, S., and Heilman, W.: Wildland fire emissions, carbon, and climate: wildfire–climate interactions, *Forest Ecol. Manag.*, 317, 80–96, doi:10.1016/j.foreco.2013.02.020, 2014. 32326

Mallet, M., Dulac, F., Formenti, P., Nabat, P., Sciare, J., Roberts, G., Pelon, J., Ancellet, G., Tanré, D., Parol, F., di Sarra, A., Alados, L., Arndt, J., Auriol, F., Blarel, L., Bourriane, T., Brogniez, G., Chazette, P., Chevaillier, S., Claeys, M., D’Anna, B., Denjean, C., Derimian, Y., Desboeufs, K., Di Iorio, T., Doussin, J.-F., Durand, P., Féron, A., Freney, E., Gaimoz, C., Goloub, P., Gómez-Amo, J. L., Granados-Muñoz, M. J., Grand, N., Hamonou, E., Jankowiak, I., Jeannot, M., Léon, J.-F., Maillé, M., Mailler, S., Meloni, D., Menut, L., Momboisse, G., Nicolas, J., Podvin, J., Pont, V., Rea, G., Renard, J.-B., Roblou, L., Schepanski, K., Schwarzenboeck, A., Sellegri, K., Sicard, M., Solmon, F., Somot, S., Torres, B., Totems, J., Triquet, S., Verdier, N., Verwaerde, C., Wenger, J., and Zapf, P.: Overview of the Chemistry-Aerosol Mediterranean Experiment/Aerosol Direct Radiative Forcing on the Mediterranean Climate (ChArMEx/ADRIMED) summer 2013 campaign, *Atmos. Chem. Phys. Discuss.*, 15, 19615–19727, doi:10.5194/acpd-15-19615-2015, 2015. 32327, 32328, 32334, 32339

Müller, D., Mattis, I., Wandinger, U., Ansmann, A., Althausen, D., and Stohl, A.: Raman lidar observations of aged Siberian and Canadian forest fire smoke in the free troposphere over Germany in 2003: microphysical particle characterization, *J. Geophys. Res.-Atmos.*, 110, D17201, doi:10.1029/2004JD005756, 2005. 32326

Müller, D., Mattis, I., Ansmann, A., Wandinger, U., Ritter, C., and Kaiser, D.: Multiwavelength Raman lidar observations of particle growth during long-range transport of forest-fire smoke in the free troposphere, *Geophys. Res. Lett.*, 34, L05803, doi:10.1029/2006GL027936, 2007. 32326

Aerosol sources during the 2013 North American biomass burning episode

G. Ancellet et al.

Title Page

Abstract

Introduction

Conclusions

References

Tables

Figures

◀

▶

◀

▶

Back

Close

Full Screen / Esc

Printer-friendly Version

Interactive Discussion



- Nisantzi, A., Mamouri, R. E., Ansmann, A., and Hadjimitsis, D.: Injection of mineral dust into the free troposphere during fire events observed with polarization lidar at Limassol, Cyprus, *Atmos. Chem. Phys.*, 14, 12155–12165, doi:10.5194/acp-14-12155-2014, 2014. 32336
- Omar, A., Winker, D., Kittaka, C., Vaughan, M., Liu, Z., Hu, Y., Trepte, C., Rogers, R., Ferrare, R., Lee, K., Kuehn, R., and Hostetler, C.: The CALIPSO Automated Aerosol Classification and Lidar Ratio Selection Algorithm, *J. Atmos. Ocean. Technol.*, 26, 1994–2014, doi:10.1175/2009JTECHA1231.1, 2009. 32330
- Paris, R., Desboeufs, K. V., Formenti, P., Nava, S., and Chou, C.: Chemical characterisation of iron in dust and biomass burning aerosols during AMMA-SOP0/DABEX: implication for iron solubility, *Atmos. Chem. Phys.*, 10, 4273–4282, doi:10.5194/acp-10-4273-2010, 2010. 32326
- Pelon, J., Flamant, C., Chazette, P., Leon, J.-F., Tanre, D., Sicard, M., and Satheesh, S. K.: Characterization of aerosol spatial distribution and optical properties over the Indian Ocean from airborne LIDAR and radiometry during INDOEX'99, *J. Geophys. Res.-Atmos.*, 107, 8029, doi:10.1029/2001JD000402, 2002. 32329
- Pelon, J., Ancellet, G., Chazette, P., Totems, J., Sicard, M., Dulac, F., Di Ioro, T., Formenti, P., and Mallet, M.: Lagrangian analysis of forest fire aerosol emissions from North America to Western Mediterranean basin during the CHARMEX 2013 summer campaign, *Geophys. Res. Abstr.*, EGU General Assembly 2015, Vienna, Austria, 11710, 2015. 32327, 32339
- Petzold, A., Weinzierl, B., Huntrieser, H., Stohl, A., Real, E., Cozic, J., Fiebig, M., Hendricks, J., Lauer, A., Law, K., Roiger, A., Schlager, H., and Weingartner, E.: Perturbation of the European free troposphere aerosol by North American forest fire plumes during the ICARTT-ITOP experiment in summer 2004, *Atmos. Chem. Phys.*, 7, 5105–5127, doi:10.5194/acp-7-5105-2007, 2007. 32327
- Schnaiter, M., Linke, C., Müller, O., Naumann, K.-H., Saathoff, H., Wagner, R., Schurath, U., and Wehner, B.: Absorption amplification of black carbon internally mixed with secondary organic aerosol, *J. Geophys. Res.-Atmos.*, 110, D19204, doi:10.1029/2005JD006046, 2005. 32326
- Stohl, A., Eckhardt, S., Forster, C., James, P., Spichtinger, N., and Seibert, P.: A replacement for simple back trajectory calculations in the interpretation of atmospheric trace substance measurements, *Atmos. Environ.*, 36, 4635–4648, doi:10.1016/S1352-2310(02)00416-8, 2002. 32331

Aerosol sources during the 2013 North American biomass burning episode

G. Ancellet et al.

Title Page

Abstract

Introduction

Conclusions

References

Tables

Figures



Back

Close

Full Screen / Esc

Printer-friendly Version

Interactive Discussion



Tesche, M., Ansmann, A., Müller, D., Althausen, D., Engelmann, R., Freudenthaler, V., and Gross, S.: Vertically resolved separation of dust and smoke over Cape Verde using multi-wavelength Raman and polarization lidars during Saharan Mineral Dust Experiment 2008, *J. Geophys. Res.: Atmospheres*, 114, D13202, doi:10.1029/2009JD011862, 2009. 32341

5 Vaughan, M. A., Powell, K. A., Winker, D. M., Hostetler, C. A., Kuehn, R. E., Hunt, W. H., Getzewich, B. J., Young, S. A., Liu, Z., and McGill, M. J.: Fully Automated Detection of Cloud and Aerosol Layers in the CALIPSO Lidar Measurements, *J. Atmos. Ocean. Technol.*, 26, 2034–2050, doi:10.1175/2009JTECHA1228.1, 2009. 32330

10 Vaughan, M. A., Garnier, A., Liu, Z., Josset, D., Hu, Y., Lee, K.-P., Hunt, W., Vernier, J.-P., Rodier, S., Pelon, J., and Winker, D.: Chaos, consternation and CALIPSO calibration: new strategies for calibrating the CALIOP 1064 nm Channel, in: Proceedings of the 26th Int. Laser Radar Conf., Porto Heli, Greece, 39–55, Alexandros Papayannis, University of Athens, Greece, 2012. 32330

15 Warneke, C., Bahreini, R., Brioude, J., Brock, C., de Gouw, J., Fahey, D., Froyd, K., Holloway, J., Middlebrook, A., Miller, L., Montzka, S., Murphy, D., Peischl, J., Ryerson, T., Schwarz, J., Spackman, J., and Veres, P.: Biomass burning in Siberia and Kazakhstan as an important source for haze over the Alaskan Arctic in April 2008, *Geophys. Res. Lett.*, 36, L02813, doi:10.1029/2008GL036194, 2009. 32326

20 Warneke, C., Froyd, K. D., Brioude, J., Bahreini, R., Brock, C. A., Cozic, J., de Gouw, J. A., Fahey, D. W., Ferrare, R., Holloway, J. S., Middlebrook, A. M., Miller, L., Montzka, S., Schwarz, J. P., Sodemann, H., Spackman, J. R., and Stohl, A.: An important contribution to springtime Arctic aerosol from biomass burning in Russia, *Geophys. Res. Lett.*, 37, L01801, doi:10.1029/2009GL041816, 2010. 32326

25 Winker, D. M., Vaughan, M. A., Omar, A., Hu, Y., Powell, K. A., Liu, Z., Hunt, W. H., and Young, S. A.: Overview of the CALIPSO Mission and CALIOP Data Processing Algorithms, *J. Atmos. Ocean. Technol.*, 26, 2310–2323, doi:10.1175/2009JTECHA1281.1, 2009. 32329, 32330

Young, S. A.: Analysis of lidar backscatter profiles in optically thin clouds, *Appl. Optics*, 34, 7019–7031, doi:10.1364/AO.34.007019, 1995. 32330

Aerosol sources during the 2013 North American biomass burning episode

G. Ancellet et al.

Title Page

Abstract

Introduction

Conclusions

References

Tables

Figures



Back

Close

Full Screen / Esc

Printer-friendly Version

Interactive Discussion



Table 1. Characteristics of the biomass burning tracer emission used for the forward FLEXPART simulation. The emitted mass is only a rough estimate explaining the use of relative mass fraction in the simulation analysis. Altitude is given a.g.l.

Aerosol Source	Release Time	Horizontal domain	Vertical range, km	Emitted mass, kg
Quebec BB	18–24 Jun 2013	–80° W/–70° W, 51° N/54° N	0–3	3×10^7
Manitoba BB	20–24 Jun 2013	–102° W/–95° W, 57° N/61° N	0–3	2.5×10^7
NWT BB	22–24 Jun 2013	–128° W/–121° W, 61° N/65° N	0–5	2×10^7
N.Alaska BB	17–19 Jun 2013	–160° W/–154° W, 60° N/64° N	0–5	1.9×10^7
S.Alaska BB	19–22 Jun 2013	–154° W/–148° W, 65° N/69° N	0–5	3.6×10^7
Colorado BB	19–22 Jun 2013	–105° W/–96° W, 37° N/41° N	0–6	5×10^7

Aerosol sources during the 2013 North American biomass burning episode

G. Ancellet et al.

Table 2. Same as Table 1 for the dust tracer emission.

Aerosol Source	Release Time	Horizontal domain	Vertical range, km	Emitted mass, kg
Dust High Plains	19–22 Jun 2013	–105° W/–99° W, 37° N/40° N	0–3	5×10^7
Dust Atlantic	20–21 Jun 2013	–60° W/–50° W, 37° N/43° N	1–5	5×10^7
Dust Atlantic	20–21 Jun 2013	–69° W/–59° W, 25° N/33° N	1–4	5×10^7
Dust Atlantic	20–21 Jun 2013	–48° W/–38° W, 25° N/33° N	1–4	5×10^7

Title Page

Abstract

Introduction

Conclusions

References

Tables

Figures



Back

Close

Full Screen / Esc

Printer-friendly Version

Interactive Discussion



Aerosol sources during the 2013 North American biomass burning episode

G. Ancellet et al.

Title Page

Abstract

Introduction

Conclusions

References

Tables

Figures



Back

Close

Full Screen / Esc

Printer-friendly Version

Interactive Discussion



Table 3. Characteristics of the aerosol layers observed in the free troposphere by the ground based lidars listed in Fig. 1 on 27 and 28 June 2013.

Lidar	Wavelength nm	Layer altitude	Time period	Scattering ratio	Depolarization ratio	Lidar ratio
Menorca	355	5–7 km	27 Jun, 00:00 UT to 28 Jun 00:00 UT	1.87 ± 0.03	< 12 %	42 ± 5 sr
Menorca	355	3–5 km	27 Jun, 00:00 UT to 28 Jun 12:00 UT	1.22 ± 0.02	< 6 %	59 ± 5 sr
Barcelona	532	5–7 km	26 Jun, 20:00 UT to 27 Jun 16:00 UT cloudy after	4.3	≈ 10 %	
Barcelona	532	3–5 km	26 Jun, 12:00 UT to 27 Jun 16:00 UT cloudy after	1.4	< 10 %	
Lampedusa	532	2–4 km	27 Jun, 08:00 UT to 27 Jun 16:00 UT	1.5 ± 0.03	< 15 %	51 ± 9 sr
Lampedusa	532	2–4 km	28 Jun, 08:00 UT to 28 Jun 14:00 UT	2.8 ± 0.04	30 %	30 ± 6 sr

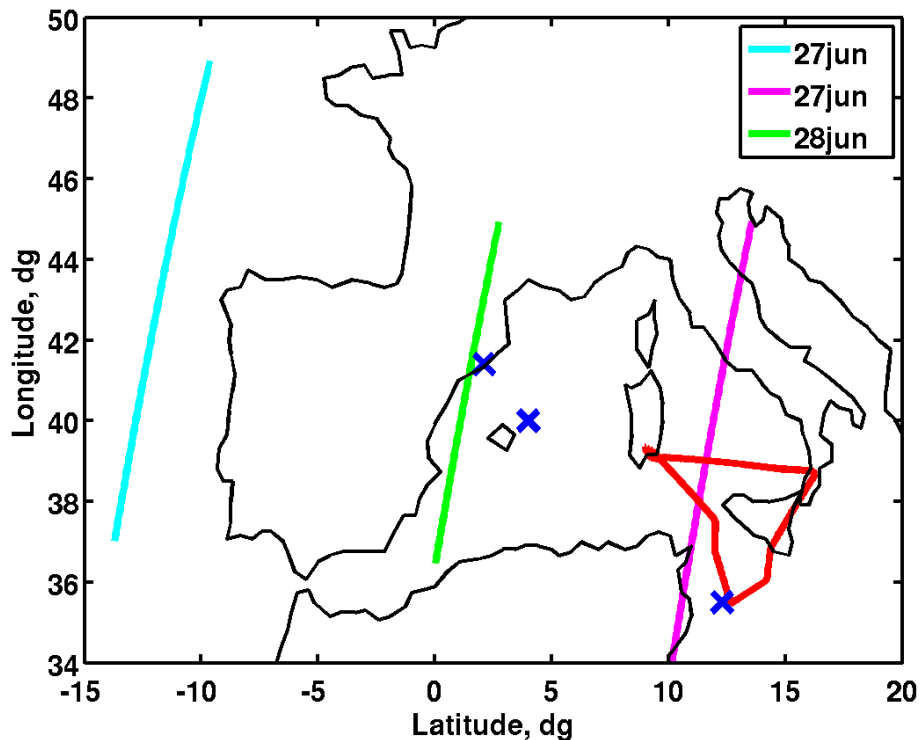


Figure 1. Map of the ChArMEx lidar observations. The colored vertical line are the positions of the nighttime CALIOP tracks on 27 and 28 June 2013. The red thick line shows the loop followed by the Falcon 20 aircraft on 28 June 2013, while the blue crosses are for the Menorca, Barcelona and Lampedusa ground based lidar.

Aerosol sources during the 2013 North American biomass burning episode

G. Ancellet et al.

Title Page

Abstract Introduction

Conclusions References

Tables Figures

◀ ▶

◀ ▶

Back Close

Full Screen / Esc

Printer-friendly Version

Interactive Discussion



Aerosol sources during the 2013 North American biomass burning episode

G. Ancellet et al.

Title Page

Abstract

Introduction

Conclusions

References

Tables

Figures



Back

Close

Full Screen / Esc

Printer-friendly Version

Interactive Discussion

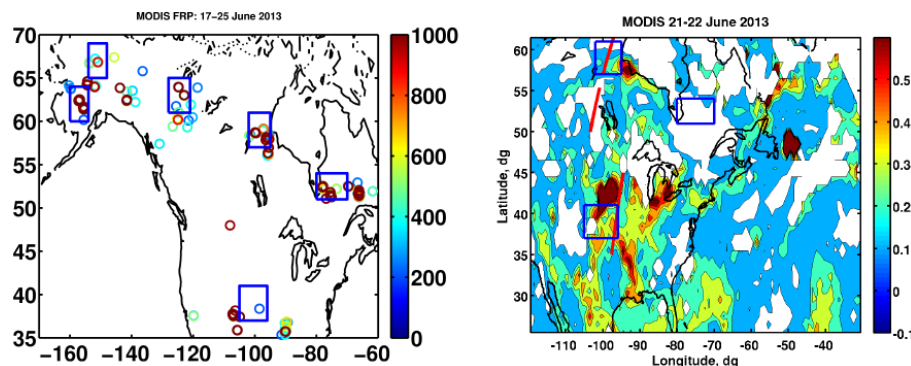


Figure 2. (Top panel) MODIS Fire Radiative Power from 17 June to 25 June. Areas with red dots are considered as significant fires. The blue boxes correspond to area chosen for the release of particles in the fire transport forward FLEXPART run. (Bottom panel) Daily AOD $0.5\ \mu\text{m}$ measured by MODIS on 22 June. The CALIOP tracks used to estimate the height of layer influenced by the fires are shown in red on 22 June near Hudson Bay fires and 21 June near Colorado fires.

Aerosol sources during the 2013 North American biomass burning episode

G. Ancellet et al.

Title Page

Abstract

Introduction

Conclusions

References

Tables

Figures

◀

▶

◀

▶

Back

Close

Full Screen / Esc

Printer-friendly Version

Interactive Discussion

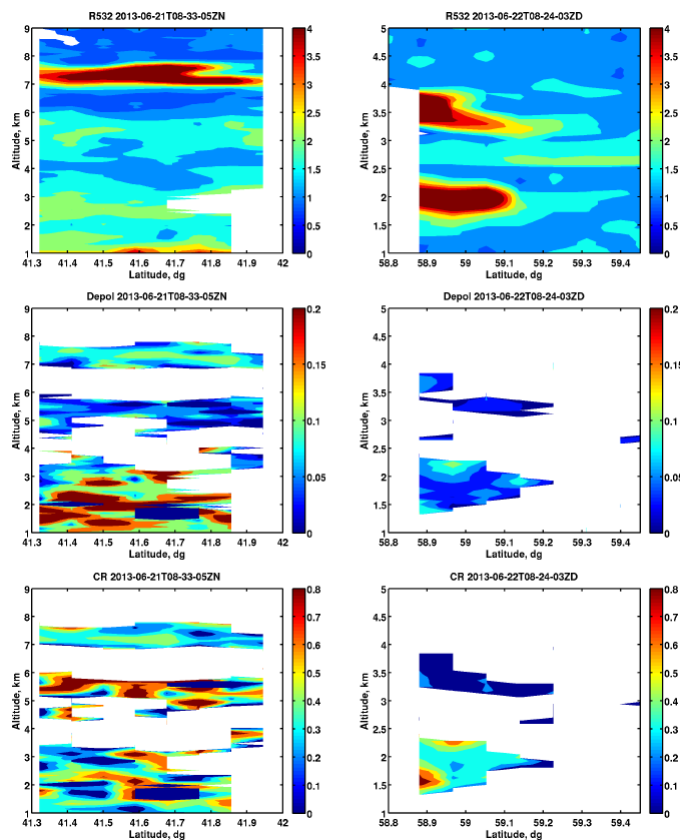


Figure 3. CALIOP vertical cross section of backscatter ratio (top), aerosol depolarization ratio (middle) and aerosol color ratio (bottom) for the two tracks shown in Fig. 2 on 21 (left) and 22 (right) June 2013. Aerosol layers on 21 June up to 8 km corresponds to the fire region over Colorado, while the layers on 22 June up to 3 km are near the Canadian fires.

Aerosol sources during the 2013 North American biomass burning episode

G. Ancellet et al.

Title Page

Abstract

Introduction

Conclusions

References

Tables

Figures

◀

▶

◀

▶

Back

Close

Full Screen / Esc

Printer-friendly Version

Interactive Discussion

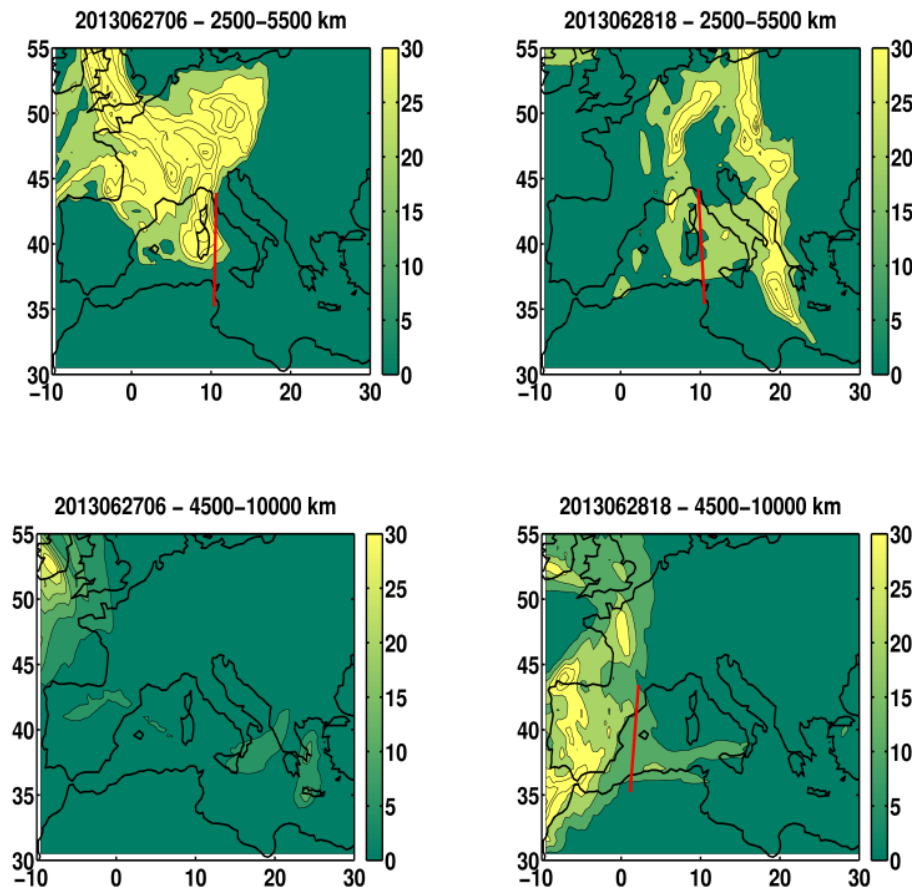


Figure 4. Map of the relative fraction of the FLEXPART biomass burning tracer plume in % for the Canadian (top) and Colorado (bottom) fires on 27 June 06:00 UT (left) and 28 June 18:00 UT (right). The altitude range corresponds to the vertical levels included in the calculation of the tracer relative fraction.

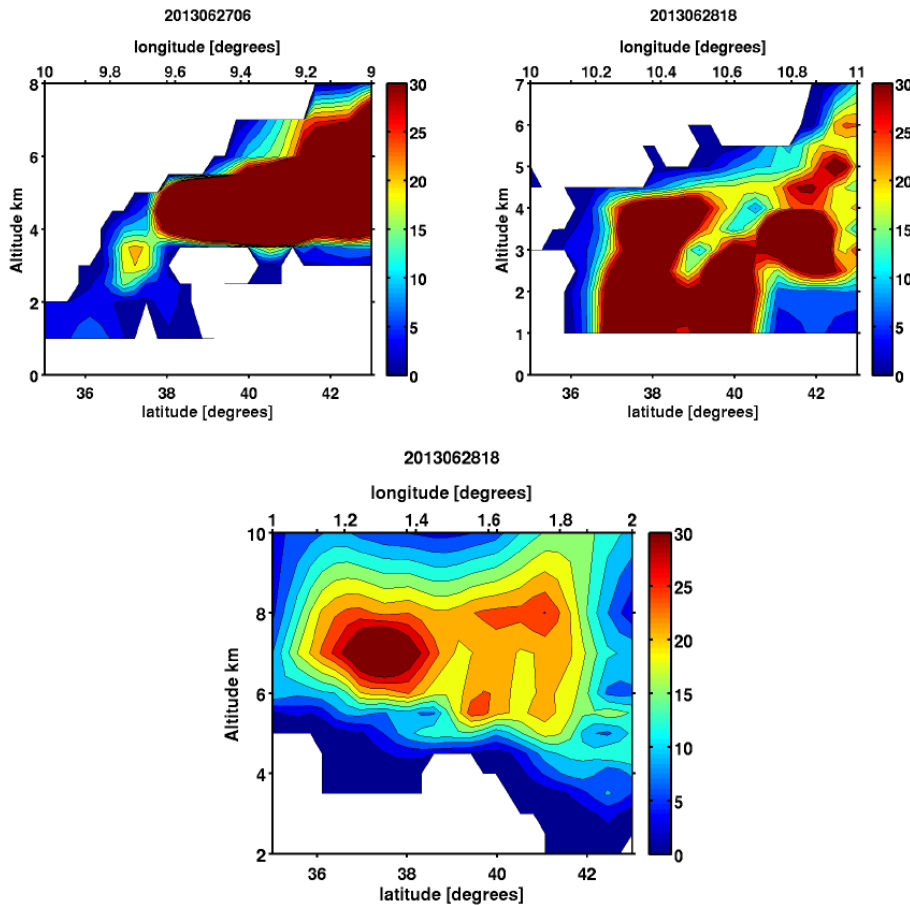


Figure 5. Vertical cross section of the relative fraction of the FLEXPART biomass burning tracer in % for the Canadian fires on 27 June, 06:00 UT (top), 28 June, 18:00 UT (middle) and the Colorado fires on 28 June, 18:00 UT (bottom).

Aerosol sources during the 2013 North American biomass burning episode

G. Ancellet et al.

Title Page	
Abstract	Introduction
Conclusions	References
Tables	Figures
◀	▶
◀	▶
Back	Close
Full Screen / Esc	
Printer-friendly Version	
Interactive Discussion	



Aerosol sources during the 2013 North American biomass burning episode

G. Ancellet et al.

Title Page

Abstract

Introduction

Conclusions

References

Tables

Figures

◀

▶

◀

▶

Back

Close

Full Screen / Esc

Printer-friendly Version

Interactive Discussion

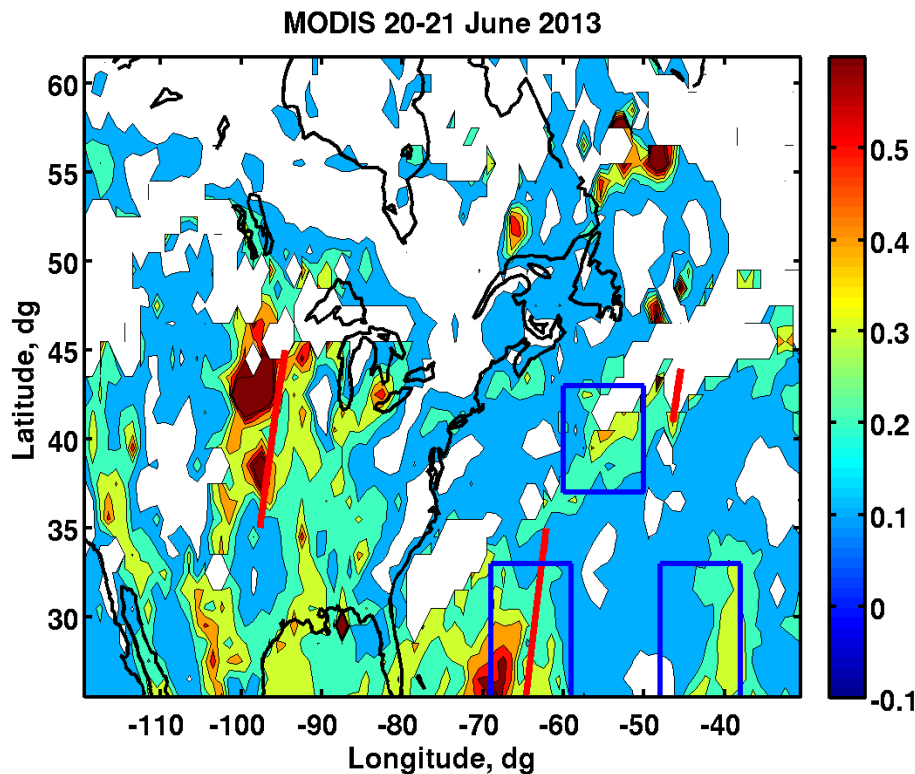


Figure 6. Daily AOD $0.5\mu\text{m}$ measured by MODIS on 20 June. The CALIOP tracks used to estimate the heights of the dust layers over the Atlantic ocean are shown in red on 20 June at 42°N and 21 June at 30°N . The blue boxes correspond to areas chosen for the release of particles in the Atlantic dust transport forward FLEXPART run.

Aerosol sources during the 2013 North American biomass burning episode

G. Ancellet et al.

Title Page

Abstract

Introduction

Conclusions

References

Tables

Figures

◀

▶

◀

▶

Back

Close

Full Screen / Esc

Printer-friendly Version

Interactive Discussion

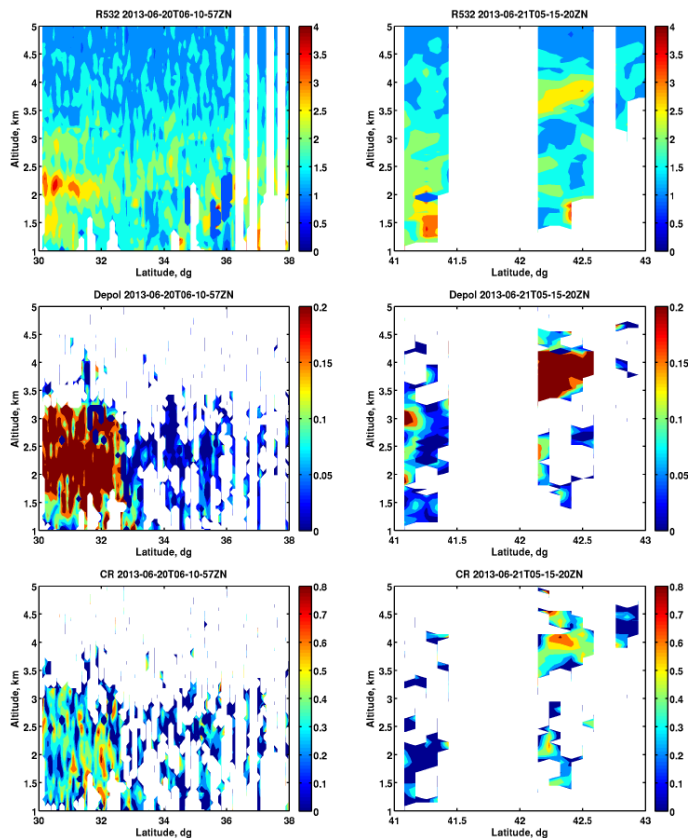


Figure 7. Same as Fig. 3 for the two tracks shown in Fig. 6 on 20 (left) and 21 (right) June 2013. Dust layers are seen above the Atlantic ocean in the altitude range 2–4 km between 30 and 34° N on 20 June and at 42° N on 21 June.

Aerosol sources
during the 2013 North
American biomass
burning episode

G. Ancellet et al.

Title Page

Abstract

Introduction

Conclusions

References

Tables

Figures

◀

▶

◀

▶

Back

Close

Full Screen / Esc

Printer-friendly Version

Interactive Discussion

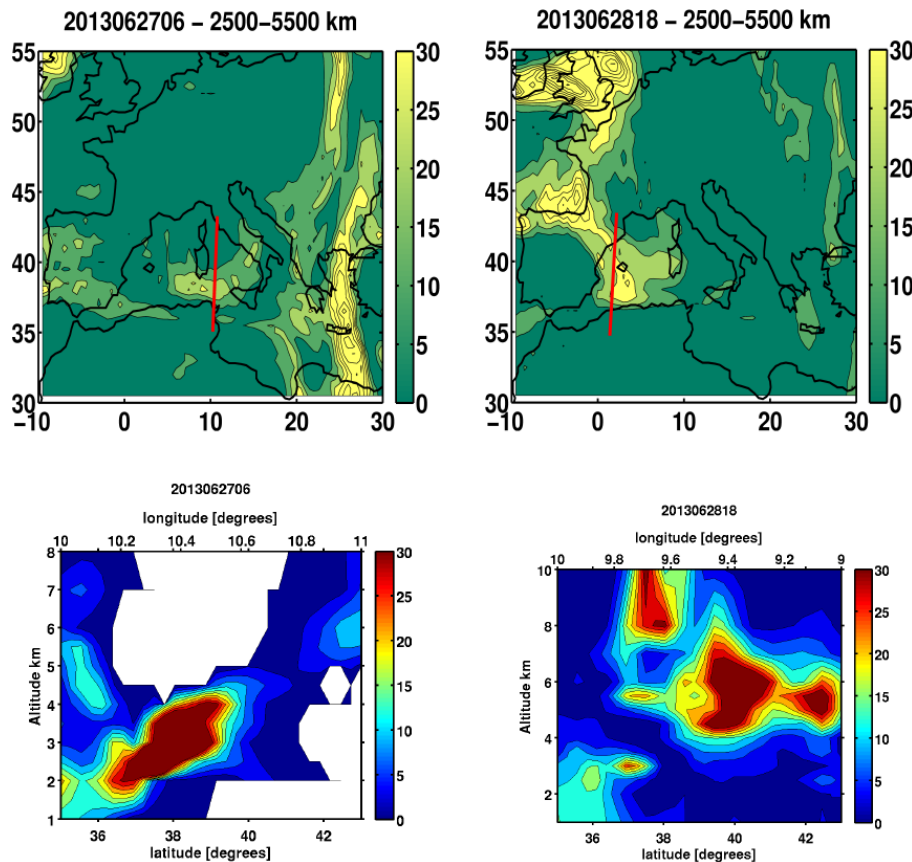


Figure 8. Map (top) and vertical cross section (bottom) of the relative fraction of the Atlantic dust tracer in % on 27 June, 06:00 UT (left) and 28 June, 18:00 UT (right). The altitude ranges in the top figures correspond to the vertical levels included in the calculation of the tracer relative fraction.

Aerosol sources during the 2013 North American biomass burning episode

G. Ancellet et al.

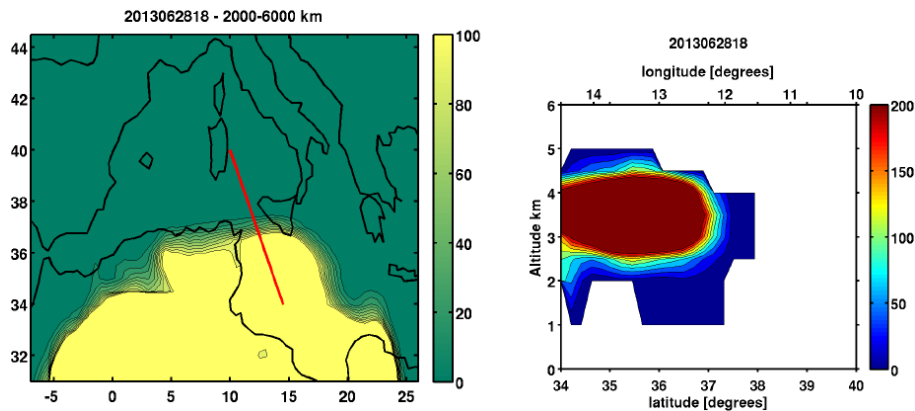
[Title Page](#)[Abstract](#)[Introduction](#)[Conclusions](#)[References](#)[Tables](#)[Figures](#)[Back](#)[Close](#)[Full Screen / Esc](#)[Printer-friendly Version](#)[Interactive Discussion](#)

Figure 9. Same as Fig. 8 for the FLEXPART Saharan tracer on 28 June, 18:00 UT.

Aerosol sources during the 2013 North American biomass burning episode

G. Ancellet et al.

Title Page

Abstract

Introduction

Conclusions

References

Tables

Figures

◀

▶

◀

▶

Back

Close

Full Screen / Esc

Printer-friendly Version

Interactive Discussion

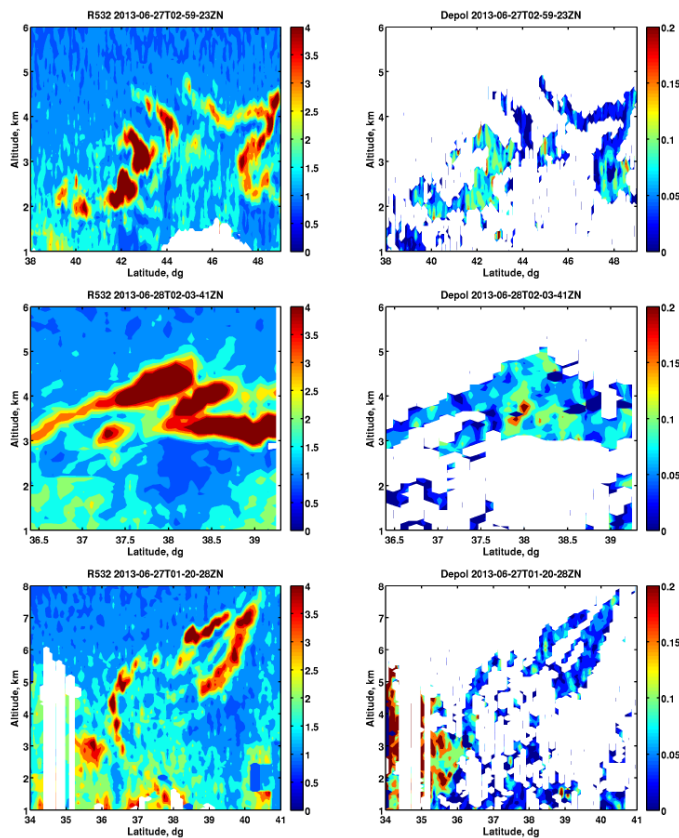


Figure 10. CALIOP vertical cross section of backscatter ratio (left panel), aerosol depolarization ratio (right panel) for the 3 tracks shown in Fig. 1 on 27 June 2013, 03:00 UT at -10° W (top panel), on 28 June 2013, 02:00 UT at 0° W (middle panel), on 27 June 2013, 01:00 UT at 10° E (bottom panel).

Aerosol sources during the 2013 North American biomass burning episode

G. Ancellet et al.

Title Page

Abstract

Introduction

Conclusions

References

Tables

Figures

◀

▶

◀

▶

Back

Close

Full Screen / Esc

Printer-friendly Version

Interactive Discussion

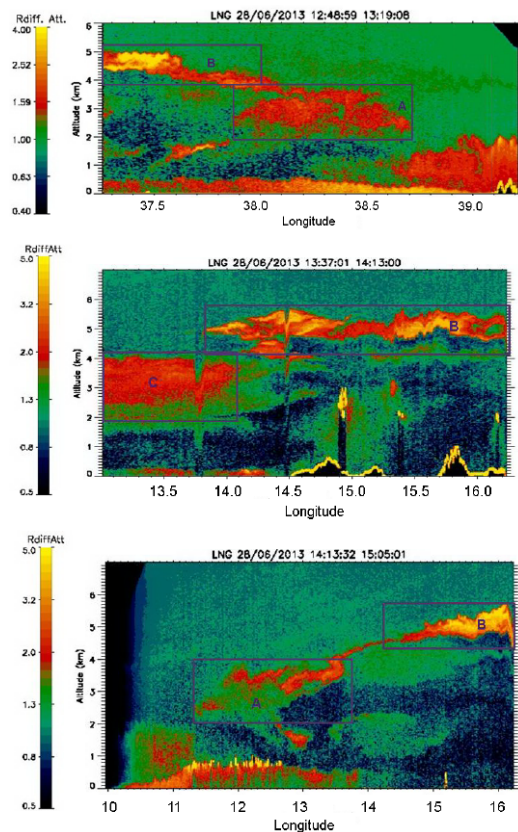


Figure 11. Airborne lidar vertical cross sections of attenuated backscatter ratio at 532 nm on 28 June along the loop shown in Fig. 1: (top) Lampedusa/Cagliari (middle) Lampedusa/Messina (bottom) Cagliari/Messina.

Aerosol sources during the 2013 North American biomass burning episode

G. Ancellet et al.

Title Page

Abstract

Introduction

Conclusions

References

Tables

Figures

◀

▶

◀

▶

Back

Close

Full Screen / Esc

Printer-friendly Version

Interactive Discussion

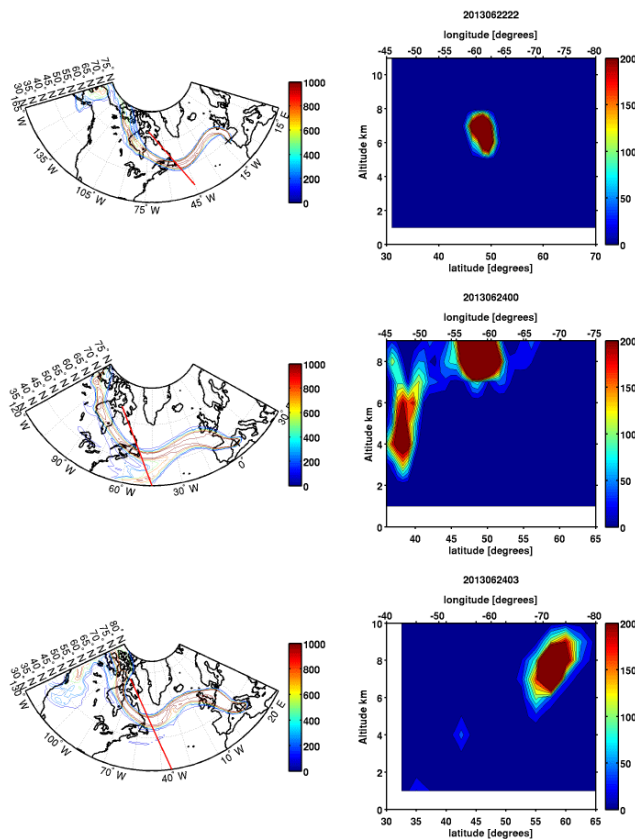


Figure 12. (Left panel) FLEXPART Potential emission sensitivity (PES) in s for 3 aerosol layers identified by CALIOP and Menorca lidar: 27 June, -10° W, 43° N (top) 27 June, 12:00 UT, in Menorca (middle) 27 June, 10° E, 39° N (bottom). The PES Vertical cross section are along the red line following the North American East Coast (right panel).

Aerosol sources during the 2013 North American biomass burning episode

G. Ancellet et al.

Title Page

Abstract

Introduction

Conclusions

References

Tables

Figures



Back

Close

Full Screen / Esc

Printer-friendly Version

Interactive Discussion

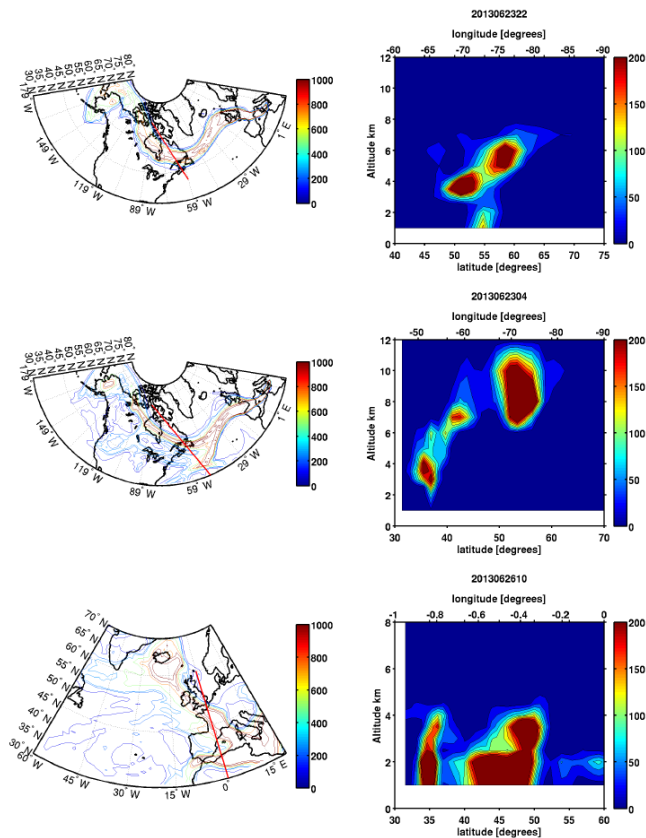


Figure 13. Same as Fig. 12 for the 3 aerosol layers identified by the Falcon 20 lidar: layer A (top) layer B (middle) layer C (bottom).

Aerosol sources during the 2013 North American biomass burning episode

G. Ancellet et al.

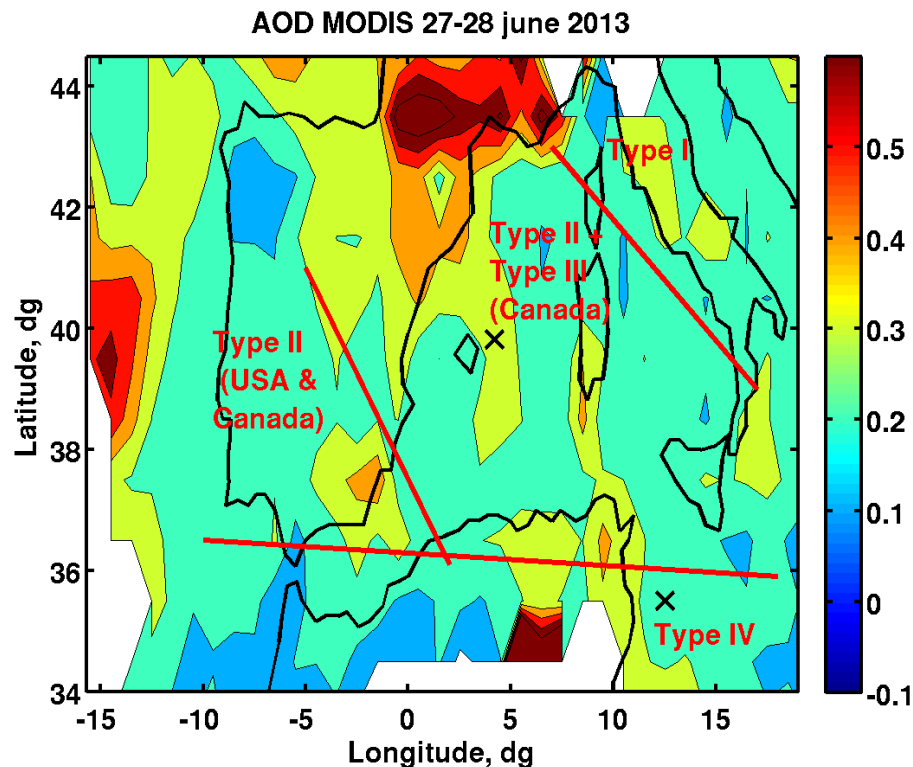


Figure 14. MODIS AOD horizontal distribution on 27 and 28 June 2008 over the Mediterranean region. The area corresponding to the aerosol types identified during our analysis of the BB plume passage are delimited by the red lines. The black crosses are for the Menorca and Lampedusa stations.